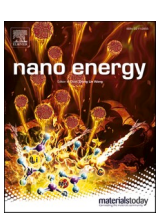
ELSEVIER

Contents lists available at ScienceDirect

Nano Energy

journal homepage: www.elsevier.com/locate/nanoen





Programming mechanoluminescent behaviors of 3D printed cellular structures

Jiayu Zhao ^a, Seongkyu Song ^c, Xuan Mu ^d, Soon Moon Jeong ^{c,e,*}, Jinhye Bae ^{a,b,f,g,**}

- ^a Department of NanoEngineering, University of California San Diego, La Jolla, CA 92093, USA
- ^b Chemical Engineering Program, University of California San Diego, La Jolla, CA 92093, USA
- ^c Division of Energy Technology, DGIST, Daegu 42988, Republic of Korea
- ^d Department of Biomedical Engineering, Tufts University, Medford, MA 02155, USA
- e Department of Interdisciplinary Engineering, DGIST, Daegu 42988, Republic of Korea
- ^f Material Science and Engineering Program, University of California San Diego, La Jolla, CA 92093, USA
- g Sustainable Power and Energy Center (SPEC), University of California San Diego, La Jolla, CA 92093, USA

ARTICLEINFO

Keywords: Mechanoluminescence 3D printing Granular materials Elastomers Stress sensors

ABSTRACT

Mechanoluminescence (ML) materials enable the transformation of mechanical stimuli into optical signals. However, current ML devices have limited luminescent programmability and mechanical tunability due to the relatively simple geometries as restricted by the conventional fabrication techniques. Here, we develop a strategy that is applicable for various types of zinc sulfide (ZnS)-based phosphors for allowing the fabrication of ML elastomer into complex 2D or 3D geometries with periodic cellular structures. We demonstrate that different cellular structures with tunable mechanical properties enable programmable structure-dependent ML behaviors including anisotropic and isotropic luminescence. We further exploit the quantitative structure-stress-luminescence relationship, which provides fundamental knowledge support for designing next-generation ML-based stress sensors and wearable devices.

1. Introduction

With the advent of the 4th industrial revolution, connecting technological advances to our daily lives requires the development of new types of devices, sensors, and robots that could adapt to new demands [1]. For instance, emerging applications such as artificial skin [2], flexible electronic devices [3], and health monitoring devices [4] require the development of the next generation of stress sensors that are stretchable, sensitive, biocompatible, and self-powered. To fulfill these requirements, ML-based sensing, which refers to the light emission process as a result of force applied [5–9], has been extensively studied in the past few decades due to its unique transduction principle from mechanical energy to photon emission [10–14].

While rigid phosphors such as quartz, sugar, rocks, alkali halides, and molecular crystals have been reported to exhibit ML phenomenon, their luminescence is not repeatable because they will be permanently damaged after emitting ML. Thus, stretchable ML materials with intense and repeatable luminescence, typically consisting of either rare-earth-

ion-doped aluminates or zinc sulfide (ZnS) embedded in a soft matrix, have been widely explored. In particular, ZnS/polydimethylsiloxane (PDMS) composites have received considerable attention due to their self-recoverable ML and biocompatible characteristics [15-18], making them a promising material system for fabricating ML-based stress sensors. Strategies have been employed to further improve the sensitivity to meet the needs of practical applications, including modification of the PDMS composition by adding nanoparticles to concentrate the stress [19] and optimization of PDMS micro-scale architecture for increasing stress conduction efficiency [10,20]. ML-based textiles fabricated by melt-spinning, coating, and weaving were developed to further push the development of novel wearable devices [21,22]. However, despite recent advances, ML characteristic has not been fully leveraged due to a lack of understanding of the structure-stress-luminescence relationships. The understanding of such relationships of ML materials has been inherently limited by the difficulty of fabricating complex and well-defined patterns or architectures using conventional methods like mold casting and coating. Previous works have reported ML devices

^{*} Corresponding author at: Division of Energy Technology, DGIST, Daegu 42988, Republic of Korea.

^{**} Corresponding author at: Department of NanoEngineering, University of California San Diego, La Jolla, CA 92093, USA. *E-mail addresses*: smjeong@dgist.ac.kr (S.M. Jeong), j3bae@ucsd.edu (J. Bae).

produced by extrusion-based 3D printing, however, their printed structures possess relatively simple geometric designs due to the lack of control over the rheological properties of ML materials [19,23]. Developing a new approach to tune the rheological properties of ML materials is necessary for extrusion-based 3D printing of complex and well-defined structures. The printed structures with periodic truss arrays could allow us to investigate structure-stress and structure-mechanical property relationships of ML devices.

Here, we demonstrate the programmable luminescent patterns using various ML cellular structures composed of periodic truss arrays with a certain arrangement by exploiting the structure-stress-luminescence relationship obtained through numerical analysis. We adopt extrusionbased 3D printing to fabricate complex 2D and 3D ML structures using a paste-like granular ZnS:Cu/PDMS ML ink with silica nanoparticles (SiNPs) and the secondary PDMS precursor (ZnS:Cu/PDMS composite ML ink). This ZnS:Cu/PDMS composite ML material is printed into periodic cellular structures with positive and negative Poisson's ratios, which alternatively give rise to anisotropic and isotropic light emission when subjected to uniaxial stretch, respectively. Finite Element Analysis (FEA) is employed to obtain the stress distribution profiles of cellular structures, which are then directly mapped with the ML profiles to reveal the structure-dependent relationship between the simulated stress and spatial intensity of ML. Moreover, tunable mechanical behavior is achieved by varying cellular structures with different Poisson's ratios. Especially, the cellular structure with a negative Poisson's ratio showcases outstanding stretchability compared to the ones with positive Poisson's ratios. We further demonstrate the use of a selfpowered optical wearable stress sensor with two different cellular structures that exhibit programmed light emission behavior in response to mechanical stress. We envision this work will provide fundamental knowledge support for the next generation of ML-based devices and sensors that require customized structure design with programmed optical properties.

2. Experimental

2.1. Preparation of printable ML inks

3D printable ML inks were prepared by the formation of the capillary state in the ZnS:Cu/PDMS composite ML ink. Briefly, the ML ink preparation consisted of three steps: ZnS:Cu/PDMS MBs synthesis, capillary state formation by adding secondary PDMS precursor, and SiNPs addition. First, ZnS:Cu/PDMS MBs were prepared by crosslinking ZnS:Cu/ PDMS emulsions in water. 3 g of PDMS base (Sylgard 184, Dow corning), 0.3 g of PDMS curing agent, and 7 g of ZnS:Cu-based phosphors (average diameter: ~25 µm) (blue: GG64, green: GG45, orange: GG13, Global Tungsten & Powders Corp.) were mixed for 1 min at 2000 rpm in a planetary mixer (Thinky mixer AR-100, Thinky Inc.). Then, 15 ML of 14 wt% polyvinyl alcohol (Mowiol 18–88, Sigma-Aldrich) aqueous solution was added and mixed for another 5 min at 2000 rpm. Next, the emulsified mixture was poured into 26 ML 85 °C deionized water while stirring at 550 rpm for 2 h to crosslink the emulsified ZnS:Cu/PDMS. The ZnS:Cu/PDMS MBs were then washed five times with 50 ML of 0.1 wt% polysorbate 20 solution (Sigma-Aldrich). In order to form the capillary state in ZnS:Cu/PDMS MBs suspension, the secondary PDMS precursor (PDMS base with curing agent at a weight ratio of 10:1) corresponding to 14 wt% of ZnS:Cu/PDMS MBs suspension was added to ZnS:Cu/PDMS MBs suspension and mixed for 2 min at 2000 rpm. After mixing, it was observed that excess water came out from the mixture due to the hydrophobicity of the secondary PDMS precursor. After removing the excess water, 1.4 wt% of SiNPs (CAB-O-SIL EH-5, size: $0.2-0.3 \mu m$) were added and mixed with the capillary ink at 2000 rpm for 3 min or longer time until the mixture reached its homogeneity (i.e., no visible aggregation of SiNPs).

2.2. 3D printing of ML materials

The ML ink was loaded to a 10 ML luer-lock syringe (Soft-Ject, Air-Tite Product) and mounted to the dispenser of the extrusion-based 3D printer (Rokit INVIVO). The ink was printed onto a glass slide (75 mm \times 50 mm \times 1 mm) from either a 20 or an 18-gauge blunt luer-lock syringe tip (0.6- and 0.8-mm inner diameter, respectively). The printing path was controlled by the G-code generated by the slicing software (New K Creator). The STL files were created using SketchUp. The secondary PDMS precursor in the printed samples was further cured at 80 °C for 30 min.

2.3. Characterization

Rheological analysis of the ZnS:Cu/PDMS MBs suspension, ZnS:Cu/ PDMS capillary ink with and without SiNPs was performed using an ARG2 rheometer (TA instruments). The viscosity measurements were set to a steady-state with a shear rate ranging from 0.1 to 100 s⁻¹. The modulus measurements were set to an oscillatory state with a shear rate ranging from 0.1 to 1000 s^{-1} . The tensile tests of the cured samples printed by ZnS:Cu/PDMS capillary ink with and without SiNPs were conducted using a universal testing machine (Instron 3342, Instron Crop.) with a 100 N load cell at the strain rate of 10 mm min⁻¹. The cyclic tensile tests of ZnS:Cu/PDMS composite were conducted using the same universal test machine at the strain rate of 342 mm min⁻¹ (equivalent to the frequency of 30 cpm) with the maximum strain set to 30%. Samples of rectangular shape (40 mm \times 10 mm \times 1.2 mm) were printed for both regular and cyclic stretching tests, the Young's modulus, energy dissipation and maximum stress loss for each condition were calculated by testing three replica samples. Scanning electron microscopy (FEI Quanta FEG 250) was used to obtain the elemental information and microstructure of the cured ML ink with and without SiNPs. Fluorescence microscopy (EVOS FL, ThermoFisher) was used to visualize and analyze the morphology of ZnS:Cu/PDMS MBs before and after adding the secondary PDMS precursor. The ZnS phosphor has autofluorescence in green color, and the secondary PDMS precursor was stained with Rhodamine B (Sigma-Aldrich) in red color. After mapping each marker component by fluorescence microscope, two color channels were merged through ImageJ software. For ML spectra, we first loaded the printed rectangular shape sample (35 mm \times 10 mm \times 1.2 mm) on the periodic mechanical stretching tester, then the light emission was collected using the combination of a spectrometer (QEPro, Ocean Optics) and a vertically aligned optical fiber equipped with a collimating lens (74-UV, Ocean Optics). All ML spectra were measured under an integrating time of 3 s. For the fatigue test of ML, the ML intensities during 5000 cycles with 30 cpm S-R rate were recorded every 100 ms by integrating the spectral intensity from 400 to 800 nm. The ML characterization was performed under 30% elongation condition from the initial length of 15 mm. Photographs of the printed samples were taken from a digital camera (EOS 70D, Canon). Stress-strain relationships of cellular structured ML samples were measured at an elongation speed of 10 mm min⁻¹ using a tensile testing machine (EZ-LX HS, Shimadzu). The ML intensity profiles for cellular structures were extracted from the luminescence images shown in Fig. 4 A to D- iii using ImageJ.

2.4. Finite element analysis

We used COMSOL Multiphysics 5.4 to develop finite element analysis-based models for studying stress under stretching. The model is based on real physical size and experimentally obtained Young's moduli. Line and point profiles are obtained by the function of Data Evaluation.

3. Results and discussion

3.1. 3D printable ZnS:Cu/PDMS composite inks

To enable extrusion-based 3D printing, two criteria must be fulfilled:

shear thinning behavior to facilitate ink extrusion from the printer nozzle, and solid-like behavior (storage modulus G^{*} > loss modulus G^{*}) to retain its shape after deposition [24]. As the simple mixture of ZnS: Cu/PDMS precursor cannot be directly printed out with shape retention due to its low viscosity ($\eta \approx 10^2~Pa\mbox{-s}$ at $10^{-1}~s^{-1}$) (figure S1), we

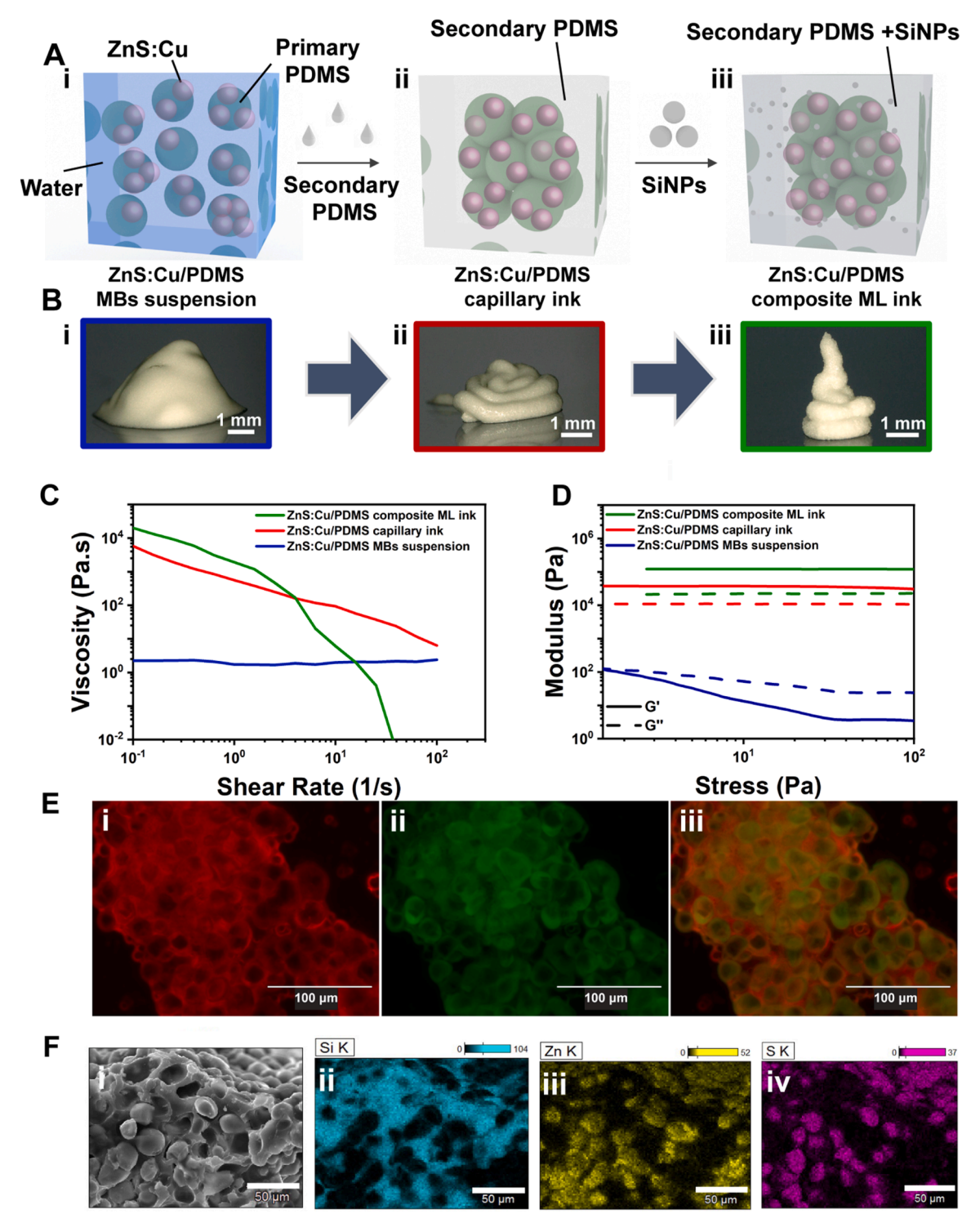


Fig. 1. Synthesis of the 3D printable ML ink. (A) Schematic illustration of the capillary ink fabrication. Secondary PDMS precursor (light grey) is added to (i) ZnS:Cu (pink)/PDMS (green) MBs suspension and mixed in a planetary mixer. After mixing, the liquid-like MBs suspension readily transforms to a (ii) paste-like capillary ink, (iii) SiNPs are further added to the capillary ink to improve rheological behavior. (B) Photographs of (i) ZnS:Cu/PDMS MBs suspension, (ii) after adding secondary PDMS precursor (ZnS:Cu/PDMS capillary ink) and (iii) after adding SiNPs (ZnS:Cu/PDMS composite ML ink. Log-log plot of (C) viscosity as a function of shear rate and (D) modulus as a function of stress. (E) (i) Red channel for visualizing the secondary PDMS precursor and (ii) green channel for visualizing the ZnS:Cu particles. (iii) composite image of ZnS:Cu/PDMS capillary ink. ZnS:Cu has autofluorescence (green) and the secondary PDMS precursor was stained with Rhodamine B (red). (F) (i) SEM and (ii to iv) EDX images of the printed ZnS:Cu/PDMS composite using the capillary ink doped with SiNPs.

developed a ML ink formulation consisting of pre-cured ZnS:Cu/PDMS microbeads (MBs), secondary PDMS precursor, and SiNPs to improve its rheological properties. Firstly, ZnS:Cu/PDMS MBs were synthesized by crosslinking the emulsified ZnS:Cu/PDMS precursor (primary PDMS) mixture in water at 80 °C for 1.5 h with magnetic stirring at 500 rpm (Fig. 1A-i). After washing and stabilizing with 0.1% (v/v) polysorbate 20 solution, the ZnS:Cu/PDMS MBs were well dispersed (figure S2A to C). The secondary PDMS precursor was further added as a surface-wetting liquid, which preferentially wet the ZnS:Cu/PDMS MBs due to the similarity of their chemical nature (Fig. 1A-ii). Lastly, SiNPs were added to the capillary ink to not only improve the printability but also enhance the light emission intensity of the printed ML device owing to the percolating network created based on the particle-particle interactions (Fig. 1A-iii) [25]. The addition of secondary PDMS precursor and SiNPs allow the transformation from a flowable suspension to a paste-like capillary ink (Fig. 1B-i to iii). Although we only tested the ML material composed of ZnS:Cu-based phosphors and PDMS, we note that the ink design principles for fulfilling the rheological requirements for 3D printing are applicable to other ML materials as well, which could potentially open the avenue for 3D printing of various kinds of ML

We then quantitatively characterize the viscosity and modulus to examine the effect of each component on rheological properties. The ZnS:Cu/PDMS MBs suspension exhibits Newtonian fluid behavior as the viscosity is independent of the shear rate. (Fig. 1 C). The addition of 14 wt% secondary PDMS readily endows the capillary ink with shear thinning behavior, where the secondary PDMS precursor can bind the

MBs through capillary force, allowing the ink to exhibit shear thinning with $\eta\approx 4000$ at $10^{-1}~s^{-1}$ and $\eta\approx 80$ at $40~s^{-1}$ (Fig. 1 C) and solid-like behavior with both G' and G" increased more than two orders of magnitude over the MBs suspension (Fig. 1D) via the network formed at capillary state, [26,27] which is confirmed by the fluorescence microscope image, in which the MBs were saturated with the secondary PDMS precursor due to the surface wetting (Fig. 1E-i to iii). Further addition of SiNPs slightly increases the viscosity, G' and G", while preserving the shear thinning properties and solid-like behavior (Fig. 1 C and D). After thermal curing, the secondary PDMS crosslinked with the primary PDMS in MBs, forming a merged PDMS matrix with dispersed ZnS:Cu particles, which is confirmed by the Scanning Electron Microscopy (SEM) (Fig. 1F-i) and Energy Dispersive Spectroscopy (EDX) (Fig. 1F- ii to iv).

3.2. ML performance and mechanism

Cyclic stretching tests have been carried out to characterize both optical and mechanical performance of the ZnS:Cu/PDMS composite. Green ML is observed while the 3D printed rectangular strip subjected to uniaxial stretching (inset image of Fig. 2 A). The green ML spectra in Fig. 2 A indicates that the emitted light intensity is increased with increasing the stretching-releasing (S-R) rate from 100 to 300 cycles per min (cpm). For practical applications, durability is one of the most important factors to consider. Thus, we carried out the cyclic stretching test for studying the fatigue characteristic of the mechanical properties and ML behaviors of the ZnS:Cu/PDMS composite. The cyclic tests were performed up to 100 cycles using a universal test machine at strain rate

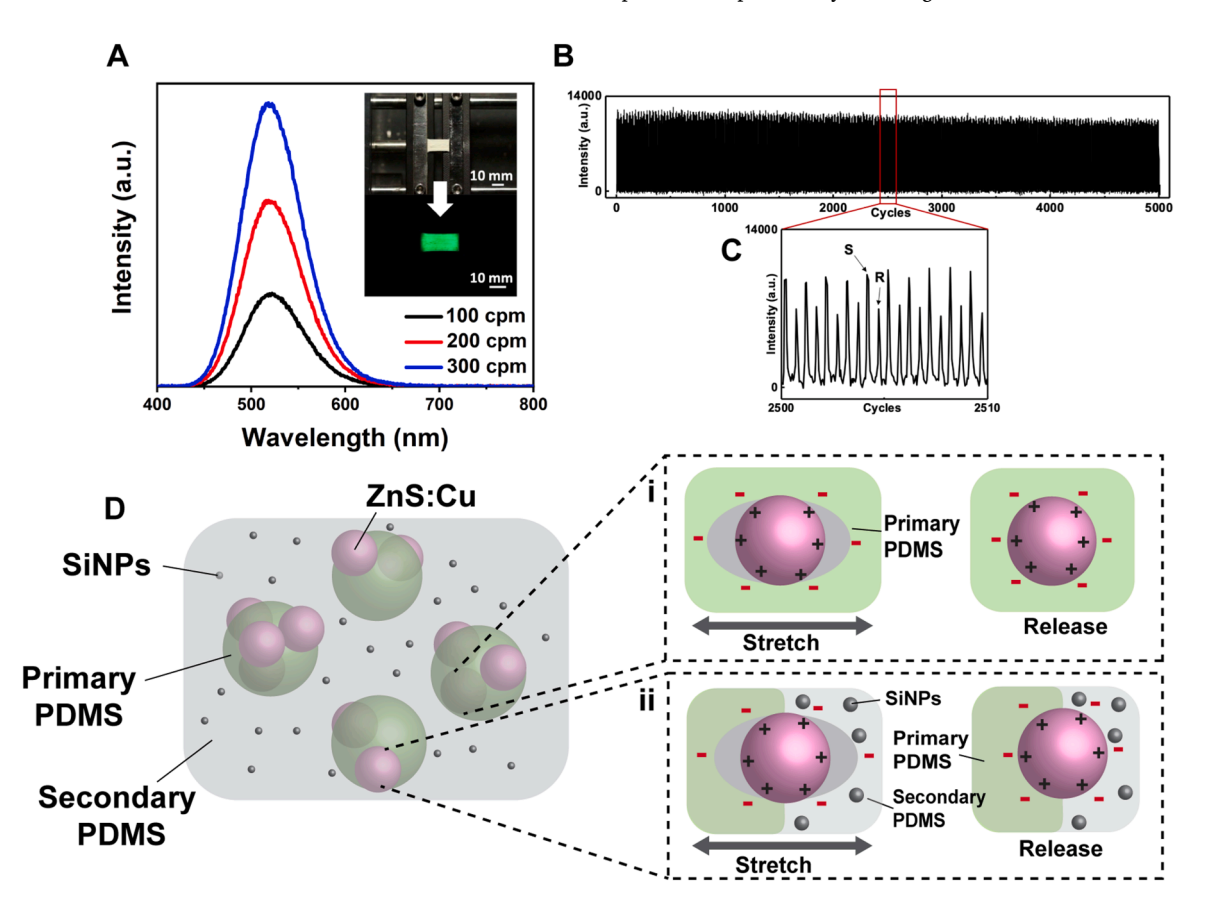


Fig. 2. Characterizations of ML optical performance and its corresponding mechanism. (A) ML spectra with increasing stretching-releasing (S-R) from 100 to 300 cpm. Inset is the photograph of an ML-emitting 3D printed rectangular strip under S-R motion (300 cpm) with 30% elongation. (B) Fatigue test of the ML intensity under cyclic stretching with the data obtained by integrating the spectral intensity in the range of 400–800 nm for 5000 S-R cycles (30 cpm). (C) The magnified plot of (B) showing two peaks appeared within one S-R cycle. (D) Schematic of the ZnS:Cu (pink)/PDMS (green) distributed in the secondary PDMS doped with SiNPs (gray). Zoom in schematic illustrating the charge distribution due to triboelectric luminescence upon stretching and releasing at two possible interfaces (i) ZnS:Cu (pink) and only primary PDMS (green); (ii) ZnS:Cu (pink) and merged PDMS matrix consisting of primary PDMS (green) and secondary PDMS doped with SiNPs (gray).

of 342 mm min⁻¹ (equivalent to 30 cpm frequency) with a constant maximum strain set to 30%. The results show that the maximum stress loss is 14 \pm 1% and 25 \pm 2% for cycles 10 and 100, respectively (figure S3), which indicates some degree of plastic deformation occurred. In addition, the displacement of loading and unloading curves indicate the ZnS:Cu/PDMS possess viscoelastic properties with an energy dissipation of 13.56 \pm 1.12 kJ m $^{-3}$ (calculation based on the area of the hysteresis loops of cycle 1 for three samples, figure S4). The printed samples exhibit stable ML intensities during the 5000 cycles of S-R motions (Fig. 2B), implying that the viscoelasticity of ZnS:Cu/PDMS composite seems to have a negligible effect on the ML intensity. A magnified plot of ML intensity as a function of the number of cycles shows that two peaks appeared in a single cycle of S-R motions, where the first and second peaks occur during the stretching and the releasing, respectively (Fig. 2 C). The non-decaying ML intensity with the increasing numbers of S-R cycle and its two peaks within one cycle has been observed in other works using the simple mixture of ZnS:Cu/PDMS [28], which are decisive evidence for the triboelectricity-induced luminescence [28,29].

Park et al. used the finite element method to show the surface potential increases as the increasing pore gap between the ZnS:Cu and the PDMS, and thus the ML intensity becomes stronger with increasing mechanical load [29]. Upon load applied, a triboelectric potential is generated by the separated interfaces (i.e., gaps) due to the deformation of the PDMS matrix, which ultimately leads to electroluminescence. In this work, there are two possible conditions that the interfaces can be created depending on whether ZnS:Cu is completely embedded in the primary PDMS or not. The first case is the interface between ZnS:Cu and only primary PDMS (Fig. 2D-i), and the second is between ZnS:Cu and the merged PDMS matrix that consists of both primary PDMS and secondary PDMS doped with SiNPs (Fig. 2D-ii), in which positively charged ZnS:Cu particles are distributed on the negatively charged PDMS surface because PDMS is relatively negative to ZnS:Cu. To verify this mechanism, we prepared control experiments and found that the printed ZnS: Cu/PDMS capillary ink without SiNPs can only emit very dim light when subjected to stretching (figure S5A), whereas the one printed with SiNPs exhibits significantly bright green light-emitting during stretching (figure S5B). In the former case, the printed ZnS:Cu/PDMS using capillary ink possesses a less uniform internal structure with micro-sized voids ranging from 200 \sim 400 μm (figure S5C), which results in the poor initial contact and subsequently dissipates the stress when subjected to an external load. Therefore, negligible triboelectric potential will be generated, leading to dim luminescence. In contrast, there are no

micro-sized voids in the sample printed with SiNPs (figure S5D), which could efficiently transfer the stress to deform the PDMS when subjected to an external load, thereby creating gaps between ZnS:Cu particles and PDMS, leading to the strong luminescence induced by triboelectricity. The SEM images indicate that the addition of SiNPs helps PDMS to adhere ZnS:Cu/PDMS MBs better compared to the one without SiNPs (figure S5E and F). This can be attributed to the similar chemical nature of PDMS and SiNPs, which helps SiNPs to be well dispersed and thus hold the PDMS matrix more tightly by the formation of percolating network. The improved adherence is attributable to the hydrogen bonding between the silanol group on SiNPs and oxygen atoms on ZnS: Cu particles.[30] As a result, the 3D printed ZnS:Cu/PDMS composite ML material exhibits enhanced mechanical properties, as indicated by the strain-stress curve shown in figure S6 with Young's modulus increased by 108% and ultimate stress increased by 10% compared to the one without SiNPs (table S1).

3.3. 3D printing of ZnS:Cu/PDMS into 2D and 3D lattice structures with multiple colors

Notably, the ML ink formulation we developed not only allows for printing of 3D lattice structure with high resolution ($\sim 100 \, \mu m$, figure S7) and good fidelity (Fig. 3 A, movie S1), but also is capable of producing various colors of ML materials by using different kinds of ZnS:Cu phosphors that can emit different colors. To directly visualize the color variation without applying mechanical stress, we irradiate the 3D printed lattice structures ($10 \times 10 \times 4 \text{ mm}^3$) with ultraviolet (UV) light so that photoluminescence of blue, green, and orange light can be emitted due to the recombination between the sulfur-vacancy-related donor and the valence band (Fig. 3B) [31]. Owing to the elasticity offered by the PDMS matrix, the 3D printed structure can be readily deformed, and the luminescence is generated by manual compression (Fig. 3 C and movie S2). In addition, we employ a dual printing technique to integrate green and orange colors of ML materials into a single 3D lattice structure ($10 \times 10 \times 4 \text{ mm}^3$) (Fig. 3D) and demonstrate that dual colors of ML can be simultaneously generated under manual compression (Fig. 3E and movie S2). We also printed a flexible 2D lattice sheet $(50 \times 50 \times 1.2 \text{ mm}^3)$ to demonstrate the concept of battery-free dual emitting fabric with green and orange colors printed perpendicular to each other (Fig. 3 F). During uniaxial stretching, the printed 2D lattice sheet emits orange and green colors with a programmable pattern defined by the printing direction (Fig. 3 J). Recently, Lewis and

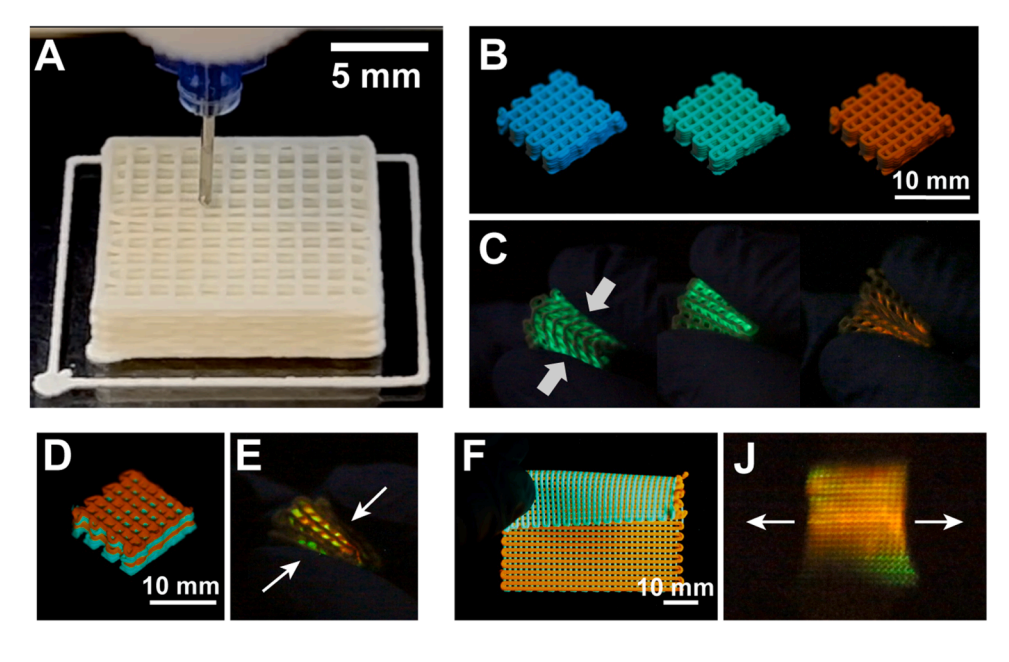


Fig. 3. 3D printing of the ML ink. (A) Photograph showing the extrusion-based 3D printing of 3D lattice structure $(15 \times 15 \times 4 \text{ mm}^3)$. Photographs of the printed ML 3D lattice structures (10 \times 10 \times 4 $mm^3) with different$ colors emitted under (B) UV irradiation and (C) manual compression, respectively. Photographs of the printed dual-color (i.e., green and orange) ML 3D lattice structure $(10 \times 10 \times 4 \text{ mm}^3)$ with interlayer design under (D) UV irradiation and (E) manual compression, respectively. Photographs of the printed 2D lattice sheet $(50 \times 50 \times 1.2 \text{ mm}^3)$ with ink containing orange ML phosphor on the top and green phosphor on the bottom under (F) UV irradiation (half of the sample is flipped to better visualize the green color at the bottom) and (J) manual stretching, respectively.

co-workers reported a multimaterial multinozzle 3D printing and showed the fabrication of voxelated soft materials [32]. We envision that the strategy we developed in this work for creating printable ML ink together with the cutting-edged printing technique can have a great impact on ML-based wearable devices, stretchable displays, and customized devices for bioimaging.

Supplementary material related to this article can be found online at doi:10.1016/j.nanoen.2022.107825.

3.4. Luminescent behavior and FEA simulation of ML cellular structures

To investigate the structure-stress-luminescence relationship using the ZnS:Cu/PDMS composite ML materials, we characterized the spatially programmed luminescence intensity by using different cellular structures. Parallel, grid and honeycomb patterns were designed (Fig. 4 A to C-i) and printed as representative cellular structures with positive Poisson's ratios (Fig. 4 A to C-ii), and an auxetic lattice was designed (Fig. 4D-i) and printed as a cellular structure with negative Poisson's ratio (Fig. 4D-ii). All the cellular structures have overall dimensions of 27-28 mm in length, 16-18 mm in width, and 1.1-1.2 mm in thickness. We note that each in the cellular structures was designed to be printed by two printing trajectories with an overall line width of ~1.5 mm so that the structures were not prone to break during the stretching test. To realize the ML auxetic pattern, we printed a 2D auxetic cellular structure consisting of the re-entrant hexagonal structure as the repeating unit (see the design and dimension information in figure S8) with a minimum theoretical Poisson's ratio of -0.51 (Fig. 4D-i and ii). However, our experimental results indicated that the Poisson's ratios of which are -0.18 and -0.03 when stretching in the x-direction at the strain of 30% and 50%, respectively (figure S9). The smaller Poisson's ratio in experiments can be attributed to the hyperelastic properties of the ZnS:Cu/PDMS composite [33], in which the applied stress serves to deform not only the overall structure but also the struts in xand y-direction that are composed of the ZnS:Cu/PDMS composite. It is also worth mentioning that if further stretch the structure to the strain of about 50%, the Poisson's ratio will become positive, at which point the re-entrant hexagonal unit cell transforms into the conventional honeycomb structure [33]. Different luminescent patterns were observed from different cellular structures when they were subjected to uniaxial stretch in the x-direction with maximum strain set to 30% (Fig. 4 A to D-iii). The photographs were taken under the same dark condition and stretching frequency, 300 cpm. (photographs of cellular structures stretched at different frequencies are provided in figure S10). The parallel line pattern emits luminescence through the stretching direction (i.e., x-direction). We note that higher intensity was observed at the position near the right and left edges than in the middle, where the color bar indicates the magnitude of the relative intensity (Fig. 4A-iii and iv), which is due to the compressive stress generated by the stretcher's grippers. Notably, the luminescence intensity of the grid structure in the x-direction is more than 300% higher compared to the y-direction (Fig. 4B-iv). This phenomenon is more obvious in the honeycomb case, in which there is almost no luminescence in the y-direction (Fig. 4C-iv). Thus, it was confirmed that the emission intensity increased according to the direction of stretching and its magnitude represents the local stress through the cellular structures. On the other hand, the auxetic cellular structure exhibits a nearly isotropic luminescent pattern through the x- and v-direction when subjected to uniaxial stretch (Fig. 4D-iv). The directional and non-directional ML patterns of cellular structures with negative and positive Poisson's ratios, respectively, can be explained by the stress distribution in the ZnS:Cu/PDMS composite matrix, as demonstrated by the FEA simulation result (Fig. 4 A to D-v). We note that the color bars on the right indicate the magnitude of the stress as a result of the applied strain (30%) in the simulation. Upon stretching, the stress generated through cellular structures with positive Poisson's ratios is mainly distributed in the x-direction same as the stretching direction, whereas the stress generated in cellular structures with negative Poisson's ratio is distributed on both x- and y-direction endowing by the arrangement of the re-entrant hexagonal cells, which leads to luminescence in both directions.

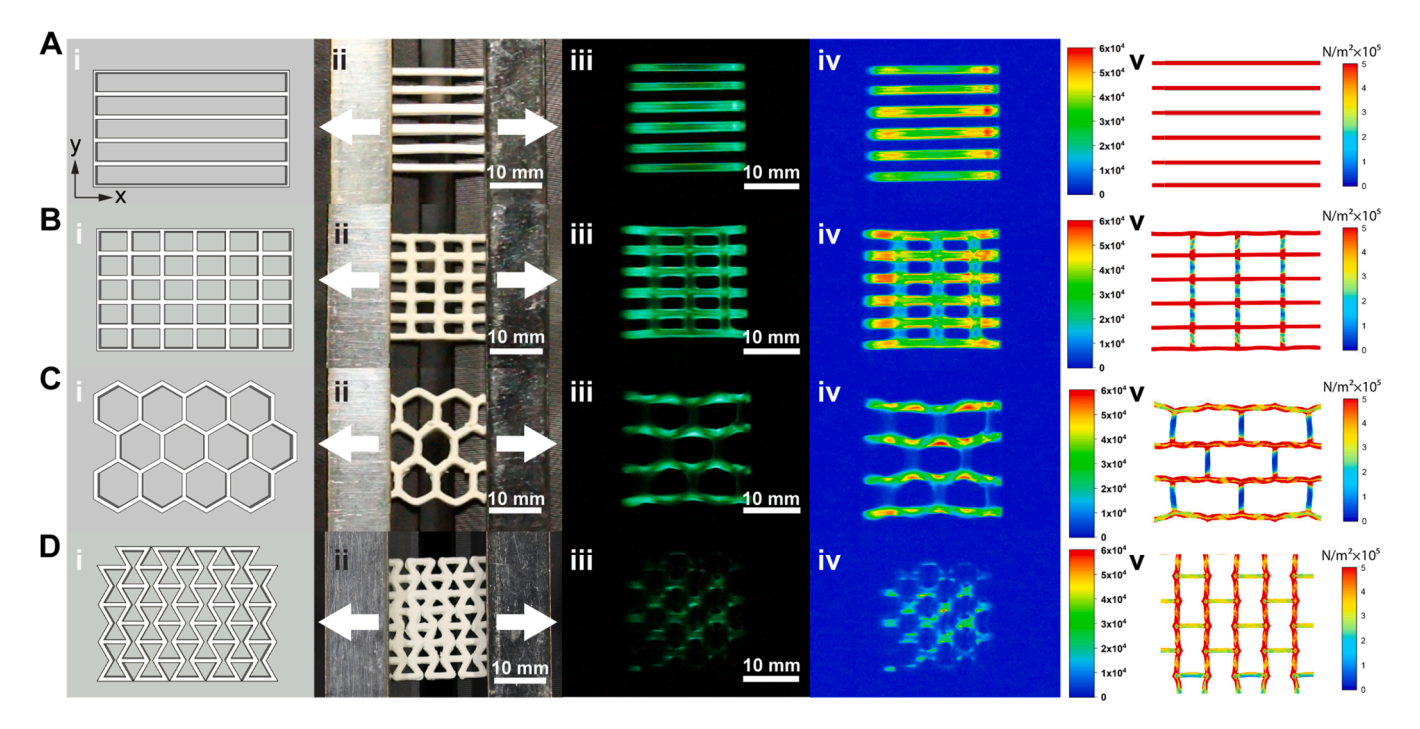


Fig. 4. ML characteristics of the printed cellular structures with positive and negative Poisson's ratios. Cellular structures of (A) parallel, (B) grid, (C) honeycomb, and (D) auxetic, respectively. (i) Top view of the 2D model for printing. (ii) Photographs of the printed cellular structures gripped on a stretcher, the arrows indicate the stretching direction. (iii) luminescent patterns under S-R (300 cpm) with 30% strain. (iv) Contour plot of the spatial distribution of ML intensity extracted from (iii). The color bar on the right indicates the intensity value. (v) FEA simulation of stress distribution subjected to 30% strain. The color bar on the right indicates the simulated stress value.

3.5. Structure-stress-luminescence-stress relationships

Linear correlation between luminescence intensity and the magnitude of applied stress has been reported using 2D film.[10] To quantitatively study the structure-dependent stress-luminescence relationship of the cellular structures, ten different spatial points were randomly

selected from each structure as shown in figure S11, and the corresponding gray values were extracted as spatial luminescent intensities from the ML profiles shown in (Fig. 4 A to D-iii) using ImageJ and plotted with the simulated stress obtained from FEA simulation (Fig. 5 A). The colored areas in Fig. 5 A indicate the 95% confidence ellipses of the ten data points for each cellular structure (see

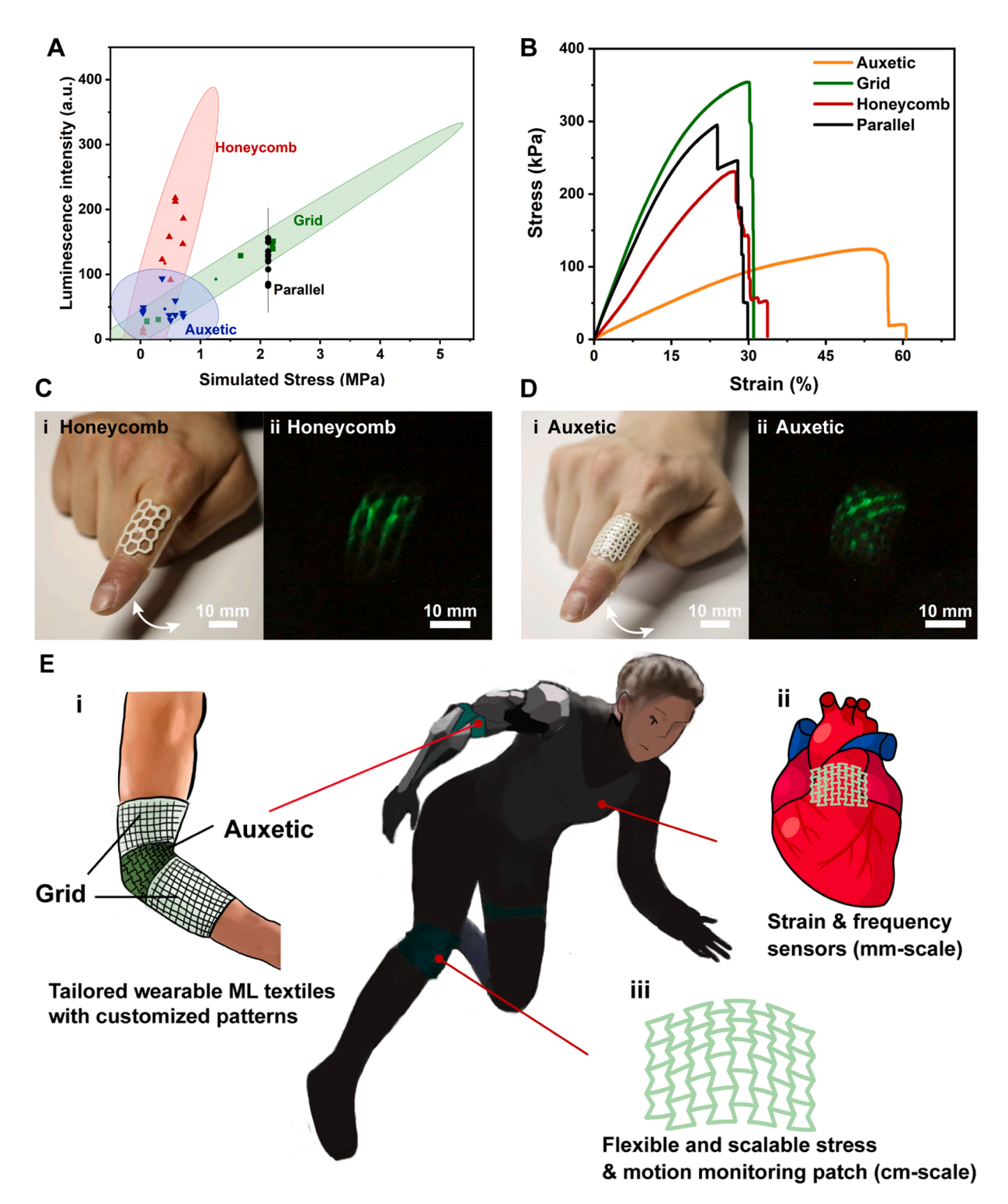


Fig. 5. Structure-stress-luminescence relationship and optical stress sensors demonstration. (A) The plot of luminescence intensity with respect to the simulated stress of parallel (black), grid (green), honeycomb (red), and auxetic (blue). The colored areas indicate the 95% confidence ellipses of the ten data points for each cellular structure. (B) Stress-strain curve for each cellular structure. Photographs of the ML-based optical stress sensor with (C) honeycomb and (D) auxetic structure attached to the index finger (i) in the light and (ii) upon finger bending in the dark. (E) Schematic of potential applications of smart ML-based materials: (i) tailored wearable ML textiles, (ii) self-powered strain and frequency sensors and (iii) flexible and scalable stress and motion monitoring patches.

supplementary text for details). The spatial luminescence intensity of the parallel line pattern ranges from 80 to 160, independent of the simulated stress (nearly 2 MPa). This variation of luminescence intensity can be attributed to the gripping effect aforementioned, which inevitably exists in the experimental condition. Ideally, we will see nearly uniform luminescence intensity through the parallel cellular structure if both ends of the sample are not gripped, because the stress is uniformly distributed in this case as the simulation shown in Fig. 4A-v. Notably, the simulated stress and luminescence intensity of honeycomb and grid structures exhibit a linear relationship, in which the luminescence intensity increases as the simulated stress increase. This correlation explains the anisotropic luminescent pattern of grid and honeycomb structures observed in the experiment, where the low stress in the y-direction (0.04 \sim 0.1 MPa) and high stress in the x-direction (0.5 \sim 2.2 MPa) result in dim and strong ML intensity, respectively. In contrast, luminescence intensity data of the auxetic structure showed a circular distribution in the lower stress regime since the stress is distributed more uniformly, indicating the luminescent intensities along the x- and y-direction fall into a narrower range compared to that of grid and honeycomb cellular structures. As a result, the normalized standard deviation of the luminescence intensity of the auxetic structure is 0.4, which is smaller than that of grid (0.6) and honeycomb structures (0.7), respectively. The auxetic structure would be particularly useful for developing optical stress sensors that are independent of stretching direction. Furthermore, the ratio of luminescence intensity and stress indicates the range of sensitivity of ML, which is $39 \sim 73$ for parallel line pattern, 63 \sim 260 for grid structure, 182 \sim 375 for honeycomb structure and 50 \sim 1025 for auxetic structure, meaning that the sensitivity can also be controlled by structural design.

The cellular structures with positive and negative Poisson's ratios not only possess distinct differences in stress-luminescence relationships but also exhibit tunable mechanical properties, making them ideal candidates for designing electronic skin or wearable sensors. Specifically, stretchability that can withstand large strains up to tens of percent is highly desired [34]. In the previous work, ML-emitting composite sheets were conventionally fabricated by incorporating rigid phosphors into PDMS, and experienced higher stress concentration by their inherent positive Poisson's ratios, which led to a relatively poor mechanical performance with limited stretchability. Geometric pattern engineering has shown to be an effective approach to tune the mechanical properties without changing the material compositions [24]. The different cellular structures that we fabricated in this work exhibit different mechanical properties with strain at break ranging from 30% to 60%, maximum stress ranging from 124 to 354 kPa, and Young's modulus ranging from 3.5 to 19 kPa (Fig. 5B). Especially, the stress-strain curves displayed in Fig. 5B highlight the outstanding flexibility of the auxetic structure, with two folds larger magnitude of strain at break compared with the ones with positive Poisson's ratio, indicating its potential to serve as a promising candidate for the wearable optical sensor that would be subject to large deformation (i.e., \sim 40% strain). We note that the strain generated due to the motion of the body may vary depending on the specific body part engaged, ranging from as low as 20% strain for facial expression or as high as 40% for finger bending [19,35], therefore, wearable devices with tunable mechanical properties that can be adapted to the specific scenario are highly desirable. As a proof of concept, we demonstrate a wearable stress sensor with a honeycomb and an auxetic structure, respectively, attached to the index finger (Fig. 5C and D-i). The stress generated by the bending of the finger is converted to a luminescent pattern. Notably, the ML emitted from the honeycomb structure is mostly localized along the bending direction of the finger (Fig. 5C-ii and movie S3), whereas the one from the auxetic structure is spatially uniform regardless of the bending direction (Fig. 5D-ii and movie S4). We anticipate that the ML-based devices with programmed luminescent behaviors and tunable mechanical properties developed in this work will pave the way for the battery-free optical stress sensor to meet a wide range of demands. In addition, ML-based tailored wearable

fibers and textiles with customized patterns as intelligent skin can be fabricated using the 3D printable ink that we developed in this work compared with the conventional weaving [22]. For instance, the grid pattern can serve as the supporting component of the smart wearable device as it possesses stronger mechanical properties, while the auxetic pattern can serve as the compliance component as it is more flexible (Fig. 5E-i). We note that the 3D printability of ML material not only allows for complex structural design but also enables the production of scalable devices, combined with the biocompatibility of the PDMS/ZnS: Cu composite [36], making it appealing in applications such as biomedical devices, in which it can be conformally attached to human body parts that would be subject to continuous deformation. For example, the 3D printed ML material with auxetic cellular pattern in mm-scale can be deployed as strain and frequency sensors on the heart or blood vessels for monitoring the pulse (Fig. 5E-ii), and the one in cm-scale can be used as a self-powered flexible patch on various body parts to monitor motion and stress (Fig. 5E-iii).

Supplementary material related to this article can be found online at doi:10.1016/j.nanoen.2022.107825.

4. Conclusion

In summary, we have demonstrated the structure-stressluminescence relationship by expanding the geometric design space for ZnS-based ML materials and the ability to produce complex 3D and 2D lattice structures using a simple yet effective strategy via extrusionbased 3D printing. The defining feature of our strategy is to create ZnS:Cu/PDMS composite printable ink that can be printed into complex 3D geometries at high resolution ($\sim 400 \, \mu m$) by tuning their rheological behaviors. We envision that with the strategy developed in this work together with the multi-nozzle 3D printing technique, more colors can be integrated into one object with programmed spatial distribution and functionality to further leverage its potential in wearable devices, stretchable displays, and electronic skin. Notably, programmed ML behavior has been demonstrated by exploring the structure-luminescence relationships of various cellular structures experimentally and computationally. The cellular structure with a negative Poisson's ratio possessed a luminescent pattern independent of stretching direction, which could be useful as an optical stress sensor that requires insensitiveness to the change of applied stress direction and spatially less localized optical signals. Furthermore, we have demonstrated that a wide range of mechanical properties can be achieved by geometric programming without changing the material chemistry and composition. We anticipate that the programmable luminescent behaviors and tunable mechanical properties will make the 3D printed MLbased material a suitable candidate for battery-free optical wearable stress sensors and user-interactive electronic skins that can be attached to different body parts subjecting to various strains.

Author contributions

J.B. and S.M.J. supervised the project. J.Z. prepared samples and performed the experiments. J.B., S.M.J. and J.Z. analyzed data. S.S. performed the optical characterization. X.M. performed the finite element analysis. All authors contributed to interpreting the results and preparing the manuscript.

CRediT authorship contribution statement

Jinhye Bae: Conceptualization, Supervision, Project administration, Resource, Formal analysis, Writing – review & editing. Soon Moon Jeong: Conceptualization, Supervision, Resource, Formal analysis, Writing – review & editing. Jiayu Zhao: Methodology, Formal analysis, Investigation, Data curation, Writing – original draft, Visualization. Seongkyu Song: Investigation, Formal analysis, Data curation. Xuan Mu: Formal analysis.

Declaration of Competing Interest

The authors declare that they have no known competing financial interests or personal relationships that could have appeared to influence the work reported in this paper.

Data Availability

Data will be made available on request.

Acknowledgments

This work is supported by the National Science Foundation through the University of California San Diego Materials Research Science and Engineering Center (UCSD MRSEC) grant DMR-2011924 (J.B., J.Z.), University of California San Diego start-up fund (J.B., J.Z.), and National Research Foundation (NRF) of Korea (NRF-2020R1A2B5B01001488) (S. M.J., S.S.). The authors thank Prof. Jesse Jokerst for allowing JZ to use the fluorescence microscope.

Appendix A. Supporting information

Supplementary data associated with this article can be found in the online version at doi:10.1016/j.nanoen.2022.107825.

References

- [1] A. Walther, Viewpoint: From responsive to adaptive and interactive materials and materials systems: a roadmap, Adv. Mater. 32 (2020) 1905111.
- [2] M.L. Hammock, A. Chortos, B.C.K. Tee, J.B.H. Tok, Z. Bao, 25th anniversary article: the evolution of electronic skin (e-skin): a brief history, design considerations, and recent progress, Adv. Mater. 25 (2013) 5997-6038.
- [3] M. Amjadi, K.-U. Kyung, I. Park, M. Sitti, Stretchable, skin-mountable, and wearable strain sensors and their potential applications: a review, Adv. Funct. Mater. 26 (2016) 1678-1698.
- [4] S. Yao, P. Swetha, Y. Zhu, Nanomaterial-enabled wearable sensors for healthcare, dv. Healthc. Mater. 7 (2018) 1700889.
- [5] F. Bacon . The advancement of learning (ed: J. Devey). P. F. Collier and Son, New York, NY, USA, 1901
- [6] F. Bacon. Novum organum (ed: J. Devey). P. F. Collier and Son, New York, NY,
- [7] B.P. Chandra. Luminescence of solids Plenum, New York, 1998.
- Y. Xie, Z. Li, Triboluminescence: recalling interest and new aspects, Chem 4 (2018) [9] J.-C. Zhang, X. Wang, G. Marriott, C.-N. Xu, Trap-controlled mechanoluminescent
- materials, Prog. Mater. Sci. 103 (2019) 678-742. [10] X. Wang, H. Zhang, R. Yu, L. Dong, D. Peng, A. Zhang, Y. Zhang, H. Liu, C. Pan, Z.
- L. Wang, Dynamic pressure mapping of personalized handwriting by a flexible sensor matrix based on the mechanoluminescence process, Adv. Mater. 27 (2015)
- [11] C.N. Xu, T. Watanabe, M. Akiyama, X.G. Zheng, Artificial skin to sense mechanical stress by visible light emission, Appl. Phys. Lett. 74 (1999) 1236-1238.
- [12] C.-N. Xu, T. Watanabe, M. Akiyama, X.-G. Zheng, Direct view of stress distribution in solid by mechanoluminescence, Appl. Phys. Lett. 74 (1999) 2414-2416.
- [13] D. Peng, B. Chen, F. Wang, Recent advances in doped mechanoluminescent phosphors, ChemPlusChem 80 (2015) 1209-1215.
- [14] H. Zhang, D. Peng, W. Wang, L. Dong, C. Pan, Mechanically induced light emission and infrared-laser-induced upconversion in the er-doped caznos multifunctional piezoelectric semiconductor for optical pressure and temperature sensing, J. Phys. Chem. C. 119 (2015) 28136–28142.
- [15] M.-C. Wong, L. Chen, M.-K. Tsang, Y. Zhang, J. Hao, Magnetic-induced luminescence from flexible composite laminates by coupling magnetic field to iezophotonic effect, Adv. Mater. 27 (2015) 4488-4495.
- [16] L. Chen, M.-C. Wong, G. Bai, W. Jie, J. Hao, White and green light emissions of flexible polymer composites under electric field and multiple strains, Nano Energy 14 (2015) 372-381.
- S.M. Jeong, S. Song, K.-I. Joo, J. Kim, S.-H. Hwang, J. Jeong, H. Kim, Bright, winddriven white mechanoluminescence from zinc sulphide microparticles embedded in a polydimethylsiloxane elastomer, Energy Environ. Sci. 7 (2014) 3338-3346.
- [18] V.K. Chandra, B.P. Chandra, P. Jha, Self-recovery of mechanoluminescence in zns: Cu and zns:Mn phosphors by trapping of drifting charge carriers, Appl. Phys. Lett. 103 (2013), 161113.
- [19] X. Qian, Z. Cai, M. Su, F. Li, W. Fang, Y. Li, X. Zhou, Q. Li, X. Feng, W. Li, X. Hu, X. Wang, C. Pan, Y. Song, Printable skin-driven mechanoluminescence devices via nanodoped matrix modification, Adv. Mater. 30 (2018), e1800291.
- [20] X. Wang, M. Que, M. Chen, X. Han, X. Li, C. Pan, Z.L. Wang, Full dynamic-range ressure sensor matrix based on optical and electrical dual-mode sensing, Adv. Mater. 29 (2017) 1605817.

- [21] S.M. Jeong, S. Song, H.-J. Seo, W.M. Choi, S.-H. Hwang, S.G. Lee, S.K. Lim, Batteryfree, human-motion-powered light-emitting fabric: mechanoluminescent textile, Adv. Sustain. Syst. 1 (2017) 1700126.
- [22] J. Zhang, L. Bao, H. Lou, J. Deng, A. Chen, Y. Hu, Z. Zhang, X. Sun, H. Peng, Flexible and stretchable mechanoluminescent fiber and fabric, J. Mater, Chem. C. 5 (2017) 8027-8032.
- [23] D.K. Patel, B.-E. Cohen, L. Etgar, S. Magdassi, Fully 2d and 3d printed anisotropic mechanoluminescent objects and their application for energy harvesting in the dark, Mater. Horiz. 5 (2018) 708-714.
- [24] R. Woo, G. Chen, J. Zhao, J. Bae, Structure-mechanical property relationships of 3d-printed porous polydimethylsiloxane, ACS Appl. Polym. Mater. 3 (2021)
- [25] H. Barthel, Surface interactions of dimethylsiloxy group-modified fumed silica, Colloids Surf. Physicochem. Eng. Asp. 101 (1995) 217-226.
- [26] E. Koos, N. Willenbacher, Capillary forces in suspension rheology, Science 331 (2011) 897–900.
- [27] S. Roh, D.P. Parekh, B. Bharti, S.D. Stoyanov, O.D. Velev, 3d printing by multiphase silicone/water capillary inks, Adv. Mater. 29 (2017) 1701554.
- [28] K.-S. Sohn, S. Timilsina, S.P. Singh, T. Choi, J.S. Kim, Mechanically driven luminescence in a zns:Cu-pdms composite, APL Mater. 4 (2016), 106102.
- [29] H.J. Park, S. Kim, J.H. Lee, H.T. Kim, W. Seung, Y. Son, T.Y. Kim, U. Khan, N. M. Park, S.W. Kim, Self-powered motion-driven triboelectric electroluminescence textile system, ACS Appl. Mater. Interfaces 11 (2019) 5200-5207.
- [30] J.-N. Paquien, J. Galy, J.-F. Gérard, A. Pouchelon, Rheological studies of fumed silica-polydimethylsiloxane suspensions, Colloids Surf. A Physicochem. Eng. Asp. 260 (2005) 165–172.
- [31] W.Q. Peng, G.W. Cong, S.C. Qu, Z.G. Wang, Synthesis and photoluminescence of zns:Cu nanoparticles, Opt. Mater. 29 (2006) 313-317.
- [32] M.A. Skylar-Scott, J. Mueller, C.W. Visser, J.A. Lewis, Voxelated soft matter via multimaterial multinozzle 3d printing, Nature 575 (2019) 330-335.
- [33] L. Gu. O. Xu. Z. Du. Analysis of tensile behaviour of hyperelastic auxetic cellular materials with re-entrant hexagonal cells, J. Text. Inst. 112 (2021) 173-186.
- [34] A. Chortos, J. Liu, Z. Bao, Pursuing prosthetic electronic skin, Nat. Mater. 15 (2016) 937–950.
- [35] M. Amiadi, Y.J. Yoon, I. Park, Ultra-stretchable and skin-mountable strain sensors using carbon nanotubes-ecoflex nanocomposites. Nanotechnology 26 (2015). 375501.
- [36] Y. Zhuang, R.J. Xie, Mechanoluminescence rebrightening the prospects of stress sensing: a review, Adv. Mater. (2021), e2005925.



Jiayu Zhao is a Ph.D. student in the Department of Nano-Engineering at the University of California San Diego. She received her B.S. in Polymer Science and Engineering at Beijing University of Chemical Technology in 2017, and her M.S. in Macromolecular Science and Engineering at Case Western Reserve University in 2019. Her research interests are stimuliresponsive soft materials with programmable behaviors.



Seongkyu Song is currently a Researcher in the Division of Energy Technology Research at DGIST. He received his M.S. degree in the Department of Chemical Engineering from Keimyung University, Republic of Korea, in 2011. His research interests are mechanoluminescence and transparent electrodes related to stretchable devices.



manufacturing.

Xuan Mu is an Assistant Professor in Biomedical Engineering at the College of Engineering, the University of Iowa. Before joining the current position, he worked at the National Center for Nanoscience and Technology (Beijing), Peking Union Medical College (PUMC, Beijing), Tufts University, and Brigham and Women's Hospital/Harvard Medical School. He received the General Electric (GE) Foundation Scholarship, Kwan-Cheng Wong postdoctoral fellowship, and PUMC Rising Star Award. He has published three book chapters and more than 35 peer-reviewed publications in journals, such as *PNAS* and *Nature Materials*. His research focuses on respiratory bioengineering, biopolymers, and sustainable polymer



Jinhye Bae is an Assistant Professor in the Department of NanoEngineering at the University of California San Diego. She received her Ph.D. in Polymer Science and Engineering at the University of Massachusetts Amherst in 2015, then worked in the School of Engineering and Applied Sciences at Harvard University as a Postdoctoral Fellow. Her research focuses on understanding the physical and chemical properties of polymeric materials to program their shape reconfiguration and responsiveness. Her research interests also include the integration of material characteristics into new structural design and fabrication approaches for applications in biomedical devices, soft robotics, actuators, and sensors.



Soon Moon Jeong is currently a Principal Researcher in the Division of Energy Technology and an Adjunct Professor in the Department of interdisciplinary engineering at DGIST. He obtained his B.S. and M.S. degrees in the Department of Metallurgical Engineering from Yonsei University; a Ph.D. in the Department of Organic and Polymeric Materials from Tokyo Institute of Technology in Japan. He worked in Nippon Oil Corporation as a Senior Researcher during 2009–2012. Then he joined the Nano & Bio Research Division of DGIST in 2012. His current research interests are the development of mechanoluminescent devices, and soft light-emitting optoelectronic devices.